Solution Structure of the Oxidized Fe_7S_8 Ferredoxin from the Thermophilic Bacterium *Bacillus schlegelii* by ^{1}H NMR Spectroscopy[†,‡]

Shigetoshi Aono,[§] Detlef Bentrop,[||] Ivano Bertini,*[,||] Antonio Donaire,[||,⊥] Claudio Luchinat,[#] Yohei Niikura,[||] and Antonio Rosato[||]

School of Materials Science, Japan Advanced Institute of Science and Technology, 15 Asahidai, Tatsunokuchi, Ishikawa 923-12, Japan, Department of Chemistry, University of Florence, Via Gino Capponi, 7, 50121 Florence, Italy, and Department of Soil Science and Plant Nutrition, University of Florence, P.le delle Cascine, 28, 50144 Florence, Italy

Received November 18, 1997; Revised Manuscript Received March 30, 1998

ABSTRACT: The solution structure of the paramagnetic seven-iron ferredoxin from *Bacillus schlegelii* in its oxidized form has been determined by ^{1}H NMR. The protein, which contains 77 amino acids, is thermostable. Seventy-two residues and 79% of all theoretically expected proton resonances have been assigned. The structure has been determined through torsion angle dynamics calculations with the program DYANA, using 966 meaningful NOEs (from a total of 1305), hydrogen bond constraints, and NMR derived dihedral angle constraints for the cluster ligating cysteines, and by using crystallographic information to build up the two clusters. Afterwards, restrained energy minimization and restrained molecular dynamics were applied to each conformer of the family. The final family of 20 structures has RMSD values from the mean structure of 0.68 Å for the backbone atoms and of 1.16 Å for all heavy atoms. The contributions to the thermal stability of the *B. schlegelii* ferredoxin are discussed by comparing the present structure to that of the less stable *Azotobacter vinelandii* ferredoxin I which is the only other available structure of a bacterial seven-iron ferredoxin. It is proposed that the hydrophobic interactions and the hydrogen bond network linking the N-terminus and the C-terminus together and a high number of salt bridges contribute to the stability.

Fe_7S_8 ferredoxins are a class of widely distributed iron−sulfur proteins containing one $[Fe_3S_4]^{+/0}$ cluster and one $[Fe_4S_4]^{2+/+}$ cluster, where the latter displays a more negative reduction potential than the former. Structural studies of bacterial Fe_7S_8 ferredoxins have been performed only for *Azotobacter vinelandii* ferredoxin I (*Av* FdI) for which several crystal structures of the wild-type and mutant proteins are known (e.g., refs *1*−*4*). Recently, the crystal structure of a zinc-containing dicluster ferredoxin from the thermoacidophilic archaeon *Sulfolobus* sp. strain 7 was reported, too. Its structural model contains two Fe_3S_4 clusters; there is however evidence from EPR, cyclic voltammetry, and quantitative iron analysis that this protein originally contains one Fe_3S_4 and one Fe_4S_4 cluster (*5*).

The physiological function of Fe_7S_8 ferredoxins remains up to now unclear although a wide variety of bacteria has been reported to contain Fe_7S_8 ferredoxins, suggesting that they play an important role. In the case of *Rhodobacter capsulatus*, the gene encoding the Fe_7S_8 ferredoxin (fdxA) cannot be disrupted by insertion mutagenesis, indicating that it has some specialized physiological function rendering it indispensable for the bacterium (*6*). Burgess and co-workers have shown recently that *Av* FdI regulates via an activation mechanism the expression of a NADPH−ferredoxin reductase (FPR) (*7*, *8*); it was also found that *Av* FdI binds specifically to FPR (*9*). However, disruption of the gene encoding *Av* FdI does not affect the growth of the bacterium (*10*). These results of genetic studies demonstrate that Fe_7S_8 ferredoxins can play different roles in different bacteria. It is unlikely that the Fe_4S_4 cluster in Fe_7S_8 ferredoxins participates in physiological redox reactions because its reduction potential is too negative. Only the Fe_3S_4 cluster in *Bacillus schlegelii* Fe_7S_8 ferredoxin (*Bs* Fd hereafter) can act as an electron carrier in the reduction of cytochrome *c* with NADPH and FNR although this reaction is not a physiological one (*11*).

In the past few years, NMR spectroscopy has proven to be a very powerful tool not only for the characterization of the various iron−sulfur clusters in ferredoxins and high-potential iron proteins (HiPIPs) (*12*−*21*) but also for the solution structure determination of these proteins (*22* and references therein, *23*, *24*). As far as Fe_7S_8 ferredoxins are concerned, NMR studies of these dicluster proteins were

[†] Supported by the European Union, TMR program, Network ERB CHRX CT94 0626 and Large-Scale Facility Grant ERBFMGECT95 0033 to I.B. and C.L., and via a fellowship to A.D., by "Comitato Biotecnologie e Biologia molecolare" of CNR, Italy, and by a Grant-in-Aid for Scientific Research on Priority Areas (09235212) from the Ministry of Education, Science, Sports, and Culture, Japan.

[‡] Coordinates of the family of 20 NMR structures and of the minimized average structure have been deposited in the Protein Data Bank (PDB ID code 1bc6 and 1bd6, respectively).

* To whom correspondence should be addressed. Tel: ++39 055 2757549. Fax: ++39 055 2757555. E-mail: bertini@lrm.fi.cnr.it.

[§] Japan Advanced Institute of Science and Technology.

[||] Department of Chemistry, University of Florence.

[⊥] Permanent address: Centro de Estudios Universitarios San Pablo, Universitat de Valencia, Montcada Valencia, Spain.

[#] Department of Soil Science and Plant Nutrition, University of Florence.

[1] Abbreviations: Fd, ferredoxin; *Bs*, *Bacillus schlegelii; Av*, *Azotobacter vinelandii*; RMSD, root-mean-square deviation; REM, restrained energy minimization; RMD, restrained molecular dynamics; ATCC, American Type Culture Collection.

S0006-2960(97)02818-3 CCC: $15.00
Published on Web 06/17/1998

concentrated on the assignment of their hyperfine-shifted resonances (*25*−*31*) and recently also on the modeling of the magnetic coupling in their $[Fe_3S_4]^+$ ($S = {}^1/_2$) clusters (*32*, *33*).

We report here the ^{1}H NMR solution structure of the thermostable Fe_7S_8 ferredoxin from *B. schlegelii* (optimal growth temperature 70 °C, according to the American Type Culture Collection (ATCC) catalog) in the oxidized (as isolated) form. The obtained structure of *Bs* Fd is compared to the homologous ferredoxin I from the mesophilic *A. vinelandii* in order to gain insight into the determinants of its high thermostability which is demonstrated by a variable temperature NMR study in this work.

The solution structure determination of an oxidized Fe_7S_8 ferredoxin is unprecedented and was achieved by extending the NMR methodology of previous structure determinations of Fe_4S_4 proteins (*22*, *23*, *34*) to the Fe_7S_8 case. In particular, a parametrization of the hyperfine shifts of the cysteinyl βCH_2 protons for the $[Fe_3S_4]^+$ cluster is introduced that allows the determination of the χ_2 dihedral angle ($Fe-S_\gamma-C_\beta-C_\alpha$) of cysteines coordinating to the $[Fe_3S_4]^+$ cluster.

MATERIALS AND METHODS

Sample Preparation. The Fe_7S_8 Fd from *Bs* was expressed in *Escherichia coli* and purified to homogeneity as described previously (*35*). The protein was dissolved in 20 mM sodium phosphate buffer at pH 6.5 in H_2O with final concentrations of 2−3.5 mM for the 2D NMR experiments. Protein samples in 99.9% D_2O solution were prepared by solvent exchange through ultrafiltration (Centricon-3 tube) with 20 mM sodium phosphate in D_2O at an uncorrected pH value of 6.5.

NMR Spectroscopy. ^{1}H NMR spectra for the structure determination were recorded at 288, 298, and 308 K on Bruker AMX 600 and DRX 500 spectrometers. Spectral windows of 13 and 60 ppm were applied, depending on the recycle time of the experiment. One-dimensional (1D) nuclear Overhauser effect (NOE) difference spectra were obtained upon selective irradiation of hyperfine shifted and fast relaxing resonances using irradiation times of 89 ms and a repetition rate of 5.6 s^{-1} according to previously described acquisition schemes (*36*, *37*). TOCSY (*38*) and clean-TOCSY (*39*) experiments with the MLEV-17 pulse sequence were performed with spin lock applied for 30, 60, and 80 ms. NOESY experiments (*40*) were recorded with mixing times in the 30−100 ms range. All these 2D spectra and a DQF-COSY (*41*) were acquired in the phase-sensitive mode with TPPI (*42*) for quadrature detection in the F_1 dimension. Typical acquisition parameters were relaxation delays of 0.8−1.4 s, 4096 data points in F_2, and 512 increments in F_1. Most of the experiments were performed in both H_2O and D_2O solution. The carrier was always set on the (residual) water resonance. When necessary, water suppression was achieved either by continuous coherent irradiation prior to the first excitation pulse (and during the mixing time in the case of NOESY spectra) or by the WATERGATE technique (*43*). The data matrixes were usually processed to a final size of 2048 × 1024 data points using shifted squared sine window functions prior to Fourier transformation. The spectra were calibrated assuming a chemical shift of 4.81 ppm for the water signal at 298 K with respect to DSS. They were processed with the standard Bruker software package and analyzed with the program XEASY (*44*).

Structure Calculations. The structure calculations were carried out according to a recently developed torsion angle dynamics (TAD) approach using the program DYANA (*45*). They were supplemented by restrained energy minimization (REM) on the 20 structures of the DYANA family with the lowest target function values followed by restrained molecular dynamics (RMD) in vacuo.

(1) TAD Calculations. DYANA generates structures from a given set of constraints employing a simulated annealing algorithm in the torsional angle space. Several types of constraints have been employed for the present work:

(i) Dipolar Connectivities. The volumes of assigned NOESY cross-peaks were converted into proton−proton distances by means of the program CALIBA (*46*) using five different classes of NOEs (*47*). Dipolar connectivities obtained through 1D NOE difference experiments were transformed into proton−proton upper distance limits using the steady-state approximation (*48*) with a rotational correlation time of 3.1 ns estimated from the Stokes−Einstein equation (*49*, *50*) assuming a molecular mass of 9.5 kDa for the Fe_7S_8 Fd from *B. schlegelii*. At later stages, to ease the assignment of NOESY cross-peaks, the structure with the lowest target function obtained from a preliminary structure calculation with a limited number of NOEs was used as an input model for NOESY back-calculation through the program CORMA (*51*). It is based on relaxation matrix calculations which allow the evaluation of NOE intensities between protons of a given structure. A single correlation time of 6 ns was used. A number of cross-peaks, which had not been identified yet, between protons whose resonances had already been assigned were predicted by the calculations. After checking for the presence of the most intense among such predicted cross-peaks in the experimental maps, new cross-peaks were assigned and the corresponding constraints used in the following DYANA calculations. About 100 NOEs were assigned in three cycles of this procedure and added to the other constraints.

(ii) Distance Constraints Derived from the Clusters. The two iron−sulfur clusters in *Bs* Fd were included in the structure computations as follows: two artificial amino acids were added to the residue library of DYANA. The first one is the same that was used for the construction of the Fe_4S_4 cluster in the solution structure determination of iso-1 high-potential iron−sulfur protein from *Ectothiorhodospira halophila* (*52*). It consists of a cysteinyl residue in which the thiol hydrogen was replaced by an iron atom at the proper distance which in turn is bound, through another covalent bond, to a sulfur atom that constitutes the "inorganic" sulfide in the cluster. This residue can be described by the formula $Cys-S_\gamma-Fe-S$. Values of bond lengths and angles in this residue were derived from the average of these parameters observed in known crystal structures of HiPIPs and ferredoxins (*52*). The second artificial residue for *Bs* Fd, necessary to obtain an Fe_3S_4 cluster, was built from the former by adding yet another covalently bonded "inorganic" sulfur atom. Thus, it is represented by the formula $Cys-S_\gamma-Fe(-S)_2$. Its bond lengths and angles (e.g., the S−Fe−S angle and the two $S_\gamma-Fe-S$ angles) were again obtained from crystallographic data on iron−sulfur proteins (*53*, *54*).

The C-terminal Fe_4S_4 cluster of *Bs* Fd was constructed from 4 residues of the first type, whereas the N-terminal Fe_3S_4 cluster was formed by one Cys−S_γ−Fe(−S)$_2$ and two Cys−S_γ−Fe−S residues linking the iron and the "inorganic" sulfur atoms through covalent bonds along the edges of the cubane. The connections between the clusters and their ligands were defined in agreement with the available structural data of homologous Fe_7S_8 proteins (*54*) (Cys 8, 16, and 49 were bound to cluster I; Cys 39, 42, 45, and 20 to cluster II). Cys 16 was represented by the special Cys−Fe(−S)$_2$ residue for the Fe_3S_4 cluster. A total of 42 upper and 42 lower distance limits between pairs of Fe, S, and S_γ atoms, respectively, were used to define the cubane cluster geometry (16 limits of each type for the Fe_3S_4 cluster and 26 for the Fe_4S_4 cluster). This is the minimum number of constraints necessary to build up the clusters with their geometry known from X-ray crystallography and does not impose any constraints on the backbone or C_β atoms of the cysteines involved. It is important to keep in mind that the chirality of the folding of the polypeptide chain around each one of the two clusters is left undefined in this approach. If the number of structural constraints is high enough, the protein will fold with the correct chirality. In the present solution structure the chirality of the polypeptide chain is observed to be the same as in the crystal structure of *Av* FdI.

(iii) Constraints Derived from Hydrogen Bonds. The criteria for the definition of a hydrogen bond in DYANA calculations were a H···O distance ≤ 2.4 Å and ±35° of deviation from linearity for the N···H···O angle. Hydrogen bonds involving sulfur atoms were considered if the H···S distance was smaller than 2.6 Å and the N···H···S angle deviated less than ±35° from linearity. A hydrogen bond detected in preliminary DYANA calculations was used as a constraint for the final DYANA run only if the HN proton was observed in D_2O spectra and if this hydrogen bond was present in more than 55% of the obtained structures. For each H···O hydrogen bond an upper distance limit of 2.4 Å was imposed (2.7 Å in the case of H···S hydrogen bonds). For the hydrogen bonds involving oxygen atoms, an additional upper distance limit of 3.3 Å and a lower distance limit of 2.6 Å for the N···O distance were imposed to keep some degree of linearity.

(iv) Dihedral Angle Constraints Derived from the Hyperfine Shifts of Cysteinyl βCH_2 Protons. χ_2 dihedral angles (Fe−S_γ−C_β−C_α) of the 4 cysteines coordinating the Fe_4S_4 cluster were determined from the hyperfine shifts of their βCH_2 protons (*55*, *56*) and used as constraints in the structure calculations, following the procedure described in ref *34*. Briefly, the hyperfine chemical shifts of the βCH_2 protons of the coordinated cysteines provide torsional constraints for the C_α−C_β−S_γ−Fe dihedral angle through the following equation (*55*, *56*):

$$\delta = a \sin^2 \theta + b \cos \theta + c$$

where θ is the dihedral angle between the plane defined by S_γ, C_β, and the observed nucleus and the plane defined by the C_β, S_γ, and Fe atoms. The values of *a*, *b*, and *c* (11.5, −2.9, and 3.7 ppm, respectively) have been previously parametrized for $[Fe_4S_4]^{2+}$ centers in ferredoxins (*20*). To select the appropriate value of θ among the possible solutions, the previously obtained stereospecific assignment of the geminal βCH_2 protons (*32*) was used.

(2) Refinement. Restrained energy minimization (REM) and molecular dynamics (RMD) of the final DYANA family of 20 structures were performed with the SANDER (*57*) module of the AMBER 4.1 program package (*58*). Only the structural restraints derived from NOE data were used in these calculations. The force-field parameters for all residues, except the clusters and the cysteine ligands to the iron atoms, were the standard AMBER "all atoms" parameters. For the iron and sulfur atoms as well as the iron-bound cysteines, the partial charges reported by Case and co-workers (*59*) were used. The energies of each of the 20 final DYANA structures and of the mean structure of the DYANA family were minimized. All of these structures were then subjected to a molecular dynamics simulation of 54.0 ps in vacuo. During the first 24 ps of the MD calculation, the system was heated from 0 to 300 K using a coupled thermal bath of 300 K with a time constant of 0.1 ps (*60*). The temperature of the system was kept constant at 300 K for the last 30 ps of the simulation. The time step was always 1.5 fs. A distance-dependent dielectric constant was used. The nonbonded interactions were evaluated with a cutoff of 1 nm, and the pair list was updated every 30 fs. The bond lengths in all RMD calculations were kept rigid by means of the SHAKE algorithm (*61*), whereas they were allowed to vary in all REM calculations. The RMD trajectories were analyzed with the program CARNAL (Ross, W. S., University of California, San Francisco). The final 30 ps of the RMD simulation of each structure was used to generate an average structure whose energy was again minimized. The obtained 20 structures represent the RMD family, and the result of the molecular dynamics refinement of the mean DYANA structure represents the mean solution structure of *Bs* Fd.

The analysis of 2D NMR spectra and the structure calculations (double-precision accuracy) were performed on IBM RISC6000/530 and PowerPC computers. All RMSD values reported in this work are from the mean structure. Unless otherwise indicated, they refer to best-fit superpositions of residues 2−74. The program MOLMOL (*62*) was used for the analysis and visualization of the obtained structures.

RESULTS

Thermal Stability of Bs Fd. The thermal stability of *Bs* Fd was evaluated qualitatively by a variable-temperature NMR study. A series of 1D ^{1}H NMR spectra at increasing temperatures was recorded and revealed the structural integrity of the protein up to 363 K as evidenced by the presence of the typical hyperfine-shifted resonances (Figure 1, signals A−E). Thus, *Bs* Fd is stable up to at least 363 K. In a similar series *Av* FdI denatured irreversibly during exposure to a temperature of 338 K (unpublished results). The factors possibly contributing to the considerably higher stability of *Bs* Fd with respect to *Av* FdI will be discussed in detail below.

Sequence-Specific Assignment. An assignment for the hyperfine-shifted resonances of oxidized (as isolated) *Bs* Fd was performed earlier (*32*). In that work, a structural model was used to identify seven out of eight signals with chemical shifts between 10.3 and 32.2 ppm in the 298 K ^{1}H NMR spectrum sequence specifically as βCH_2 protons of six

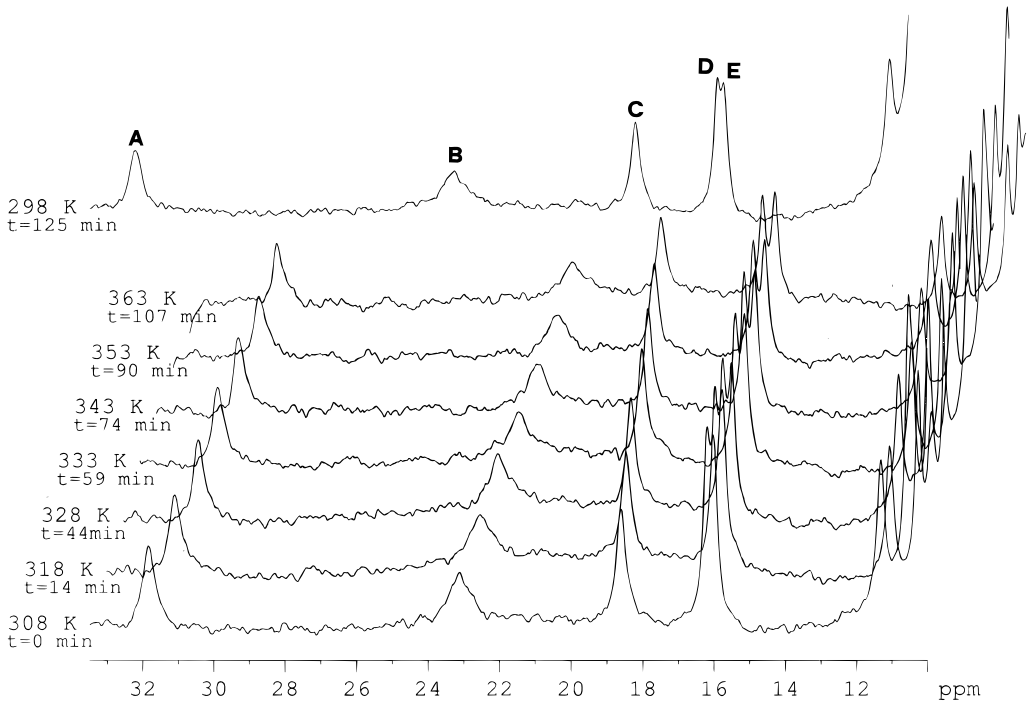

FIGURE 1: *B. schlegelii* Fe_7S_8 ferredoxin is stable up to 363 K as shown by a variable temperature NMR study. The downfield portions of ^{1}H NMR spectra (recorded with a standard one pulse sequence) at temperatures ranging from 308 to 363 K are depicted in a stacked plot. The time between the single spectra is indicated. The top trace is the spectrum at 298 K after returning to room temperature with the most shifted resonances labeled as signals A−E (*32*).

cysteines coordinating to the two clusters. Only Cys 8, the first ligand to the Fe_3S_4 cluster, escaped detection. In the present work, an extensive assignment of the proton resonances of *Bs* Fd was achieved using standard procedures via sequential NOEs between spin systems (*47*), dipolar connectivities from 1D NOE difference spectra on the hyperfine-shifted resonances, and backcalculation of NOE cross-peaks by CORMA (*51*) as an additional guideline for a few assignments. The 1D NOE difference spectra and a reference 1D ^{1}H NMR spectrum of oxidized *Bs* Fd are provided as Supporting Information (Figure S1).

The analysis and combination of information from COSY, TOCSY, and NOESY spectra recorded at 288 and 298 K allowed the unambiguous identification of the sequential stretches Tyr 2-Thr 5, Glu 6-Pro 7, Ile 9-Thr 11, Val 17-Val 19, Ile 25-Val 38, Ala 47-Val 48, and Ile 54-Lys 77 (Figure 2). In addition, a glycine spin system was assigned as Gly 43 by exclusion. The aliphatic part of the Tyr 2 spin system was assigned without intraresidual scalar connectivities on the basis of NOE cross-peaks only. At this point an extension of the assignment was achieved mainly by analysis of the 1D NOE difference spectra. The resulting connectivities permitted the assignment of protons that were matching the available structural data. The previously derived structural model (*32*) or alternatively a family of structures calculated by DYANA from the set of NOEs provided by the assignment available at this step can be used. This family of structures has a backbone RMSD of 1.44 Å and is thus sufficiently well defined to serve as an aid to the assignment of missing residues in an iterative process. The two processes, that is, with or without the use of the previous structural model, lead to the same assignments, examples of which are briefly described below.

Asp 23 was sequence specifically identified by 1D NOEs of its backbone protons with Cys 20 Hβ_2 (signal H in ref

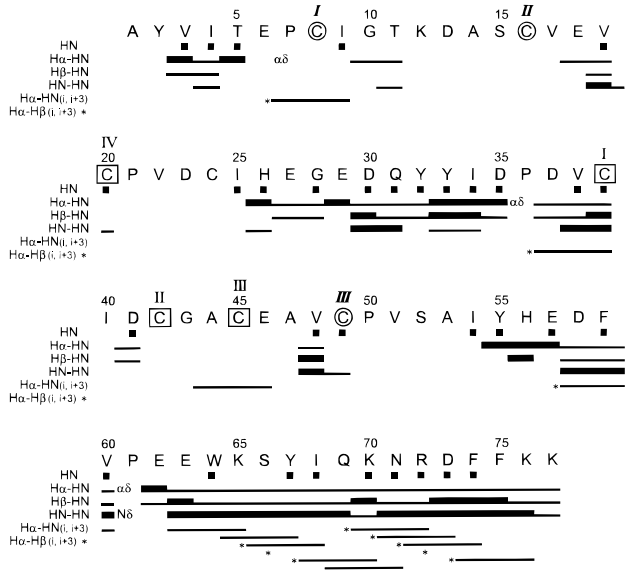

FIGURE 2: Amino acid sequence and pattern of sequential and (*i*, *i* + 3) NOEs involving HN, Hα, and Hβ protons in the Fe_7S_8 ferredoxin from *B. schlegelii*. The cysteines ligating the Fe_3S_4 cluster (C8, 16, and 49) are indicated by circles and numbered by bold-italic roman numerals in agreement with their position in the sequence. For the Fe_4S_4 cluster, the coordinating cysteines (C39, 42, 45, and 20) are indicated by squares and numbered as I−IV reflecting the pseudo-2-fold symmetry of dicluster ferredoxins. The relative NOE intensity is indicated by the width of the bars in the diagram. The asterisk (∗) indicates a Hα-Hβ NOE between the residue at the position of the asterisk (*i*) and the residue in sequence position *i* + 3 relative to it. Filled squares represent slowly exchanging backbone HN protons.

32). Cys 20, the distant cysteine of the C-terminal Fe_4S_4 cluster, is followed by a turn which brings the Hα of amino acid *i* + 3 close to the side chain of the cluster ligand. This structural feature is highly conserved in all known ferredoxins

and was also exploited for the assignment of Ser 52 through its 1D NOE connectivities with the βCH_2 protons of Cys 49 (signals A and B in ref *32*). A valine spin system whose HN was not detectable was then attributed to Val 51 due to a NOE between one of its methyl groups and HN Ser 52. Pro 21 could be assigned on the basis of dipolar connectivities with Cys 20 that were expected from the structural data. A second DYANA family of structures with a backbone RMSD of 1.27 Å was then generated with the new assignments and NOE constraints available at this point. Cys 24, the only cysteine residue of *Bs* Fd which does not coordinate to an iron−sulfur cluster, was identified by long-range NOEs with residues Asp 35 and Val 38 using the structural information.

The 1D NOE difference spectrum on signal G of *Bs* Fd (*32* and Supporting Information) provided the key information for the assignment of Ile 40 and Asp 41, the two amino acids located between the first and second cysteine of the Fe_4S_4 cluster. It shows dipolar connectivities of G to an AMX spin system (Hα 5.34 ppm; Hβ 3.47, 3.13 ppm) and to another spin system with the Hα proton at 5.27 ppm and side chain resonances at 2.77 and 1.14 ppm. The last two resonances were assigned to the side chain of Ile 40 as they are also present in the 1D NOE difference spectrum on Cys 42 Hβ_2 (signal E in ref *32*), in agreement with the expected dipolar connectivities of this proton. Thus, the above-mentioned AMX spin system was assigned to Asp 41 and signal G to HN Asp 41. An alanine-type spin system without detectable HN was assigned to Ala 1 on the basis of a 1D NOE with Cys 39 Hβ_1 (signal F in the 1D ^{1}H NMR spectrum of *Bs* Fd (*32*)) and on the basis of long-range NOEs with Pro 36 as expected for this residue from the structural data. The observed dipolar connectivity of signal G (HN Asp 41) with Hα Ala 1 is consistent with this assignment. A spin system with a downfield-shifted Hα and without detectable HN that showed a single interresidual NOE to one of the methyl groups of Val 51 was tentatively assigned as Pro 50. An incomplete spin system consisting of a HN and a side chain resonance was tentatively assigned to Glu 46 due to NOE connectivities to the side chain of Ile 54 expected from the structural data and CORMA backcalculation of NOEs.

At this point, the residues Cys 8, Lys 12-Ser 15, Val 22, Ala 44, and Ala 53 are not assigned. The 1D NOE difference spectra on the two Hβ protons of Cys 49 (signals A and B in ref *32*) allow the tentative assignment of HN Ala 53 to a resonance at 8.00 ppm; similarly, a methyl group of Val 22 can be assigned to a resonance at 1.16 ppm in the 1D NOE difference spectrum of Cys 39 Hβ_1 (signal F in ref *32*). No further assignments for these two residues can be deduced from our ^{1}H NMR spectra. Four more spin systems without detectable HN and without interresidual NOEs are visible in the TOCSY spectra. One of these spin systems has a Hα chemical shift of 3.80 ppm and Hβ's at 3.67 and 3.58 ppm. Since the latter two shifts are in the typical range of serine βCH_2 protons, this spin system was tentatively assigned to the only remaining serine in the *Bs* Fd sequence, Ser 15. An alanine-type pattern (Hα 3.95 ppm, Hβ 1.12 ppm) among the unassigned spin systems must account for Ala 14, Ala 44, or Ala 53. The remaining two spin patterns are characterized by downfield-shifted Hα protons (at 5.04 and 5.15 ppm, respectively) and are apparently of the AMX type; however, it is evident from the exclusion principle that at least one of them must be incomplete. In summary, the sequential stretch Lys 12-Ala 14 in the loop between the first and second cysteine ligands to the Fe_3S_4 cluster (ground state $S = {}^1/_2$) as well as the residues Cys 8 and Ala 44 remain unassigned.

A full list of the obtained assignments for *Bs* Fd is provided as Supporting Information (Table S1). The previous assignments of the hyperfine-shifted resonances of *Bs* Fd and of the cluster coordinating cysteines (*32*) were confirmed and extended in the present work. Overall, 79% of all theoretically expected proton resonances have been assigned. With the exception of Ser 15 that would have provided only one intraresidual NOE, all the assignments described above were used for the structure determination. As far as the tentative assignments based on dipolar connectivities expected from the available structural information are concerned, they did not lead to NOE violations in the structure calculations; this gave a posteriori strong support to them.

Angular Dependence of the Hyperfine Shifts of the Cysteinyl βCH_2 Protons of the $[Fe_3S_4]^+$ Cluster. The dependence of the hyperfine shifts of the βCH_2 protons of the cysteines coordinating to $[Fe_4S_4]^{2+}$ clusters on the Fe−S_γ−C_β−H_β dihedral angle (θ) has been deeply investigated (*55*, *56*, *63*), and its use for solution structure determination is now established (*23*, *34*) (see also Materials and Methods). To apply the same approach to the $[Fe_3S_4]^+$ cluster case, the relationship between the hyperfine shift and the dihedral angle needs to be re-parametrized. The present case is intrinsically more difficult than that of the $[Fe_4S_4]^{2+}$ cluster due to the inequivalence of the three iron ions demonstrated through ^{1}H NMR spectroscopy. With some approximation, it is possible to assume that the hyperfine shifts for the first two cluster-bound cysteines in the sequence (Cys 8 and 16 in the present work) have the same angular dependence, whereas the third one (Cys 49) has a different one. This is in agreement with the opposite temperature dependence of these two groups of signals (*12*, *14*, *32*, *33*).

In analogy to the $[Fe_4S_4]^{2+}$ case, dihedral angle values have been measured, after adding hydrogen atoms with the program MOLMOL (*62*), for the Fe−S_γ−C_β−H_β angles in the crystal structures of *Av* Fe_7S_8 FdI (*2*, *54*) and *Desulfovibrio gigas* Fe_3S_4 ferredoxin (*53*); these are the only two Fe_3S_4 containing ferredoxins for which both NMR and structural data are available. The observed hyperfine shifts have been plotted against the measured dihedral angle values, keeping the data relative to the first two cysteines separated from those relative to the third one (see above). These data points have been fitted to the same function used in the case of the $[Fe_4S_4]^{2+}$ cluster:

$$\delta = a \sin^2 \theta + b \cos \theta + c$$

where the three parameters *a*, *b*, and *c* are allowed to vary. The fit of the data points relative to the first two cysteines yielded the following parameter values: $a = 23.0 \pm 4.0$ ppm, $b = 1.0 \pm 1.3$ ppm, and $c = 2.8 \pm 1.6$ ppm, whereas for the points relative to the third cysteine, values of $a = -12.9 \pm 6.7$ ppm, $b = -2.3 \pm 1.0$ ppm, and $c = 27.8 \pm 1.9$ ppm were obtained. The above values show remarkable differences between the two groups of cysteines: *a* is positive and much larger than *c* for the first group, while it is negative

and smaller than c in absolute value for the second group. This difference implies that the angular dependence of the hyperfine shift is very strong for the first group of cysteines, whereas it is fairly weak for the second group. Regarding the second group, let us consider that the above equation can be rewritten as:

$$\delta = -a\cos^2\theta + b\cos\theta + (c - a)$$

In this way the sign of the first term becomes positive, consistent with the fact that the presence of unpaired electron spin density on a cysteinyl Hβ proton in this system yields a positive hyperfine shift. The term dominating the angular dependence of the hyperfine shift is thus of $\cos^2$ type, which implies that in this case the dominant mechanism for electron spin delocalization is due to the overlap between the 1s orbital of the hydrogen and the Fe−S σ bond. On the other hand, the $\sin^2$ dependence observed for the first group of cysteines (and for all the four equivalent cysteines coordinating to the $[Fe_4S_4]^{2+}$ cluster) implies that here spin delocalization occurs more efficiently through the overlap of the 1s orbital with one p orbital of the sulfur.

Structure Determination. A total of 1248 upper distance limits were obtained from the analysis of NOESY spectra. Fifty-seven additional dipolar connectivities were determined from 1D NOE difference spectra recorded upon saturation of the hyperfine-shifted resonances. Together with the 42 upper distance limits derived from the topology of the two clusters and the 32 upper limits from hydrogen bonds, a total of 1379 upper limits were used as input for the structure calculations. The number of meaningful distance constraints in the DYANA calculations was 1097 (i.e., 14.2/residue), or 966 (i.e., 12.5/residue) when only the NOE derived upper distance limits are taken in consideration. The structures from preliminary DYANA calculations were used as input for the auxiliary program GLOMSA (*46*) which provided a total of 41 stereospecific assignments. Finally, a χ_2 dihedral angle constraint for each of the four cysteines coordinating to the $[Fe_4S_4]^{2+}$ cluster in *Bs* Fd was determined from the hyperfine shifts of their βCH_2 protons. By means of the newly introduced parametrization for the $[Fe_3S_4]^+$ cluster, the χ_2 dihedral angles of Cys 16 and Cys 49 were determined to be −110° and 80°, respectively (the βCH_2 protons of Cys 8 are not detected). All six χ_2 angles were given a ±30° indetermination in the DYANA calculations. A summary of the structural constraints used in the present work is given in Table 1.

The final DYANA family consisted of 20 structures without consistent constraint violations and a target function below 0.86 Å^2 (average target function: 0.76 ± 0.07 Å^2). There was no NOE violation bigger than 0.28 Å^2. The RMSD from the mean structure within this family was 0.70 ± 0.12 Å for the backbone and 1.11 ± 0.10 Å for all heavy atoms; these values drop to 0.53 ± 0.12 Å for the backbone and 0.88 ± 0.11 Å for all heavy atoms when the unrestrained amino acids Lys 12-Ser 15 are excluded from the best-fit superposition. Figure 3 shows a plot of the number of NOEs per residue versus the residue number. The paucity of NOEs for amino acids in the vicinity of the coordinating cysteines is evident. This is due to the strongly enhanced relaxation introduced by the paramagnetic iron−sulfur clusters and the concomitant lack of assignments. The RMSD per residue for both backbone and heavy atoms is plotted in Figure 4 for a superposition of residues 2−11 and 16−74.

Table 1: Type and Number of Constraints for the Structure Calculations of *B. schlegelii* Fe_7S_8 Ferredoxin

NOESY distance constraints	1248
1D NOEs	57
upper limits for the clusters	42 (16 for $[Fe_3S_4]^+$, 26 for $[Fe_4S_4]^{2+}$)
lower limits for the clusters	42
hydrogen bond constraints (15 H···O and 2 H···S_γ bonds)	47
upper limits	32
lower limits	15
total no. of meaningful distance constraints[a]	1097
intraresidual	260
sequential	224
medium-range	284
long-range	329
χ_2 dihedral angle constraints	6 (2 for $[Fe_3S_4]^+$, 4 for $[Fe_4S_4]^{2+}$)
stereospecific assignments[b]	41

[a] Medium-range NOEs are between residue i and residues $i + n$ ($2 \le n \le 5$). Long-range constraints are between residue i and residues $i + m$ ($m > 5$). [b] Obtained from the program GLOMSA (*46*).

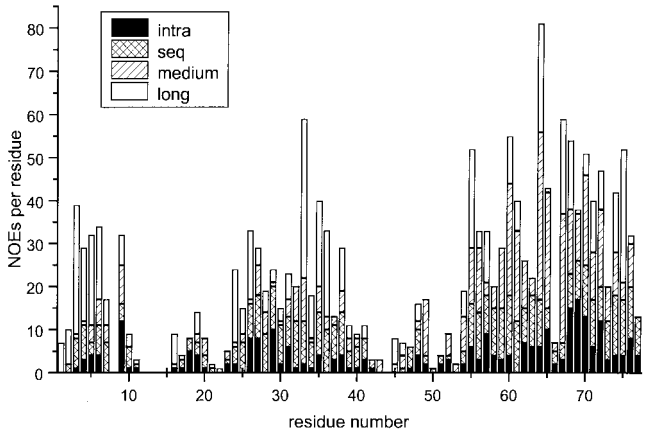

FIGURE 3: Plot of the number of meaningful intraresidual, sequential, medium-range, and long-range NOEs per residue versus the amino acid sequence.

Restrained energy minimization (REM) and molecular dynamics (RMD) were applied to the DYANA family. The RMSD from the mean structure within the REM family is almost identical to that obtained for the DYANA family: 0.69 ± 0.13 Å for the backbone and 1.12 ± 0.10 Å for all heavy atoms (or 0.51 ± 0.13 Å for backbone and 0.88 ± 0.12 Å for heavy atoms for a superposition of residues 2−11 and 16−74). The global RMSD values for the RMD family were 0.68 ± 0.13 Å for the backbone and 1.16 ± 0.13 Å for all heavy atoms (backbone RMSD of 0.51 ± 0.10 Å and heavy atoms RMSD of 0.93 ± 0.12 Å for a superposition of residues 2−11 and 16−74). The RMSD/residue for both the REM and the RMD family is also shown in Figure 4. From these plots, it can be seen that there are RMSD maxima for residues Gly 10-Ser 15, and, much less pronounced, for Val 17-Glu 18, Asp 23, Asp 30-Gln 31, Cys 42-Ala 44, and Pro 50-Ser 52 correlating with minima in the plot of NOEs per residue (Figure 3). Residues Gly 10-Ser 15 form the loop between the first and second cysteine ligand of the

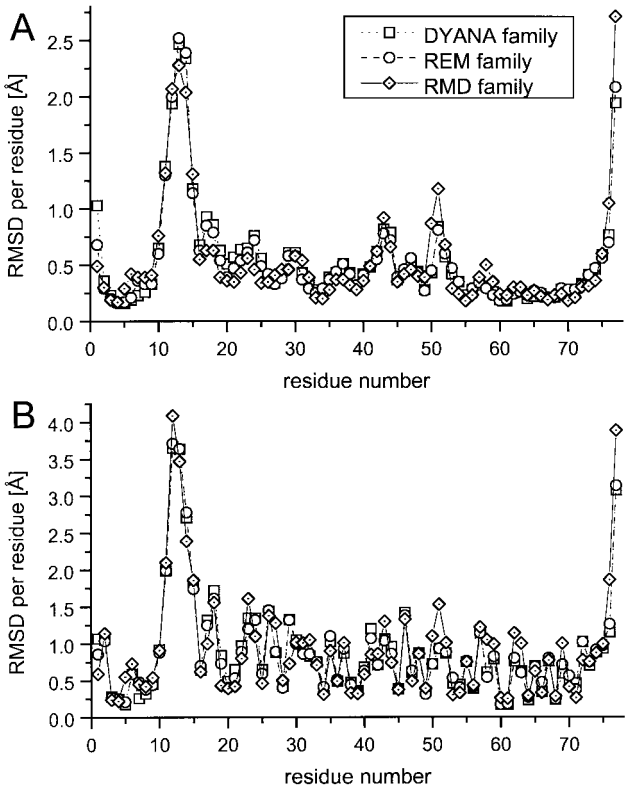

FIGURE 4: Diagram of the RMSD per residue for the backbone (A) and all heavy atoms (B) in the final family of 20 structures of *B. schlegelii* Fe_7S_8 ferredoxin from DYANA (open squares), REM (open circles), and RMD (diamonds). In all three cases, the structures were superimposed on residues 2−11 and 16−74.

Table 2: Overview of Experimental Constraint Violations in the RMD Family of *B. schlegelii* Fe_7S_8 Ferredoxin

average distance penalty function	97.0 ± 13.4 kJ/mol[a]
root-mean-square violation per NOE constraint[b]	
intraresidual	0.0375 ± 0.0037 Å
sequential	0.0203 ± 0.0024 Å
medium range	0.0150 ± 0.0025 Å
long range	0.0210 ± 0.0039 Å
total	0.0251 ± 0.0019 Å
average number of NOE violations >0.05 Å per structure[b]	
intraresidual	21.9 ± 2.6
sequential	10.1 ± 1.9
medium-range	7.7 ± 1.7
long-range	10.2 ± 2.1
total	49.9 ± 4.6
average number of NOE violations >0.3 Å/structure	0.05 ± 0.2
largest residual NOE violation	0.42 Å
average number of χ_2 violations >5° per structure	0.0

[a] Corresponding to a DYANA target function of 0.73 ± 0.10 Å^2. [b] Medium-range NOEs are between residue i and residues $i + n$ ($2 \leq n \leq 5$). Long-range constraints are between residue i and residues $i + m$ ($m > 5$).

$[Fe_3S_4]^+$ cluster. In this undefined region, a description and discussion of structural details is not possible.

Assessment of the Quality of the Structure. A summary of the violations of the experimental constraints in the final RMD calculations is reported in Table 2. On average less than 5% of the NOE constraints are violated by 0.05 Å or more in each structure. It is noted that long-range constraints account only for one-fifth of the average number of NOE violations, while the number of these constraints is roughly one-third of the total. This indicates that the obtained structure is in excellent agreement with the experimental information gathered from long-range NOEs, and guarantees that the calibration of this class of constraints, which are the most important in determining the tertiary structure of the protein, was not too restrictive. Finally, it is pointed out that the cysteine χ_2 constraints obtained from the hyperfine shifts of the βCH_2 protons were satisfied in all the conformers of the final family. Indeed, the χ_2 angles measured in a family of structures calculated without dihedral angle constraints were already in overall good agreement with the values obtained from the parametrization. The introduction of the new constraints yields a further improvement in the definition of the cysteine side chains.

Table 3: Ramachandran Plot Statistics for *B. schlegelii* Fe_7S_8 Ferredoxin[a]

	RMD family	mean structure
percentage of residues in:		
most favored regions	74.0	76.1
additional allowed regions	21.8	22.4
generously allowed regions	2.3	0.0
disallowed regions	1.9	1.5

[a] Values are reported for an analysis including all 77 residues.

The present results constitute an a posteriori validation of the new parametrization for the $[Fe_3S_4]^+$ cluster, thus supporting the general procedure outlined above. In addition, our results show that, within the limits of the sensitivity of the hyperfine shifts to the electronic structure of the iron−sulfur clusters, the latter structure is conserved in all ferredoxins. Since it is reasonable to assume that the electronic structure of the cluster would be sizeably affected by even small variations in its geometry, it can be deduced that also the latter is conserved in different ferredoxins, thus showing little dependence on its environment. This constitutes a validation of the procedure with which the cluster topology has been introduced into the solution structure calculations. The looseness with which the cluster geometry has been defined here is probably higher than the possible differences in cluster geometry observed in the solid state. This implies that no artificial restrictions were imposed in transferring the geometry of the clusters from a crystal to the present structure.

A Ramachandran plot was determined by the program PROCHECK-NMR (*64*) for the final RMD family and the mean solution structure of *Bs* Fd (see Table 3 for the percentages of residues in the four classes of Ramachandran regions). As far as the mean structure is concerned there are no residues in the generously allowed regions, and the unassigned Lys 12 is the only residue in a disallowed region.

The above structural statistics clearly demonstrate that the obtained ensemble of structures is of high quality except for the sequential stretch Gly 10-Ser 15 which is located at the surface of the protein and strongly influenced by the paramagnetism of the $[Fe_3S_4]^+$ cluster. The following discussion of structural details and issues of thermostability will be limited to the regions of the protein that are well-defined by NOEs (Figures 3 and 4).

Description of the Structure. Figure 5 shows a superposition of the backbone atoms of the 20 structures of the final

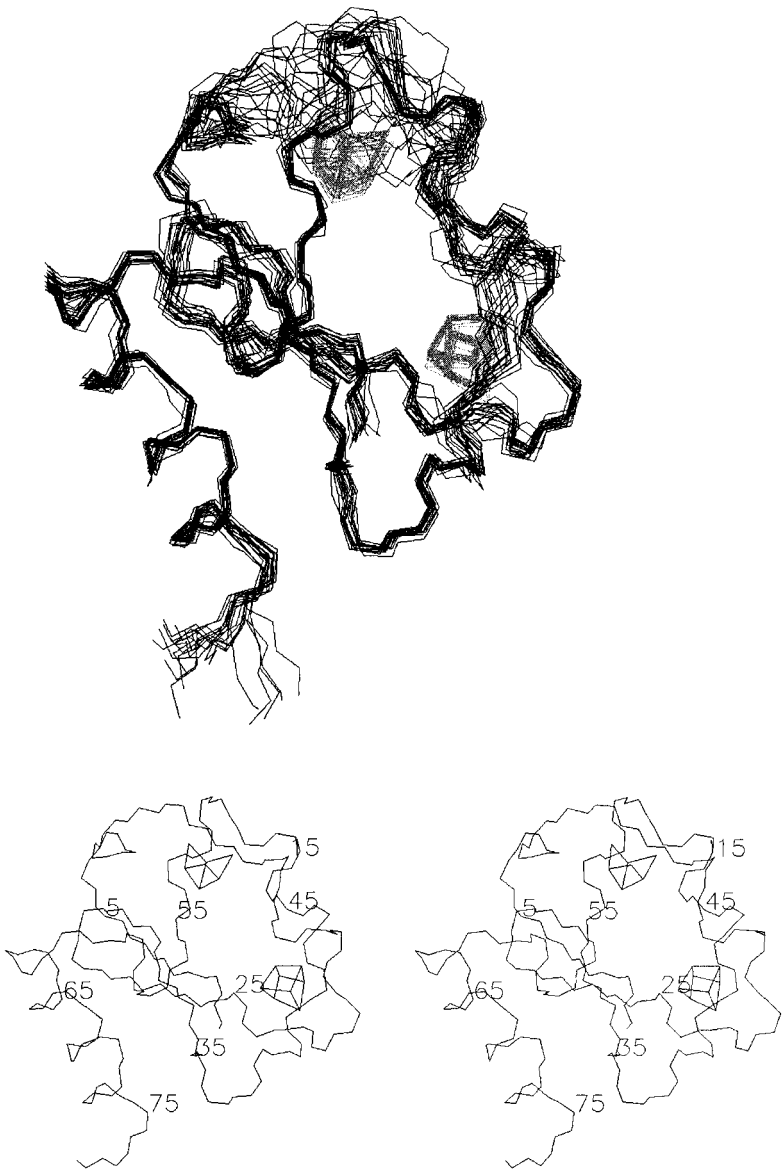

FIGURE 5: Top: A superposition of the backbone of the RMD family (20 conformers) describing the solution structure of *B. schlegelii* Fe_7S_8 ferredoxin. The two clusters are also shown (in gray). Bottom: A stereoview of the first conformer of the family.

RMD family (obtained by best fitting the coordinates of the backbone atoms of residues 2−74). A schematic drawing of the energy minimized mean solution structure of *Bs* Fd in a ribbon representation, highlighting the secondary structure elements and the two iron−sulfur clusters, is depicted in Figure 6A. The folding topology is very similar to other dicluster ferredoxins of known structure, as anticipated from the high sequence homology to these proteins (e.g., 49% sequence identity to *Av* FdI). The typical secondary structure elements of bacterial dicluster ferredoxins, present in *Bs* Fd, are (i) a short antiparallel β-sheet (β1) involving the N-terminus (Tyr 2-Val 3) and residues Tyr 55-His 56 (corresponding to the C-terminus in *Clostridium pasteurianum*, *Clostridium acidi-urici*, and *Peptostreptococcus asaccharolyticus* Fe_8S_8 ferredoxins), (ii) another two-stranded antiparallel β-sheet (β2) formed by residues Ile 25-Glu 27 and Tyr 32-Ile 34 which are sequentially located between the two cluster binding motifs, and (iii) a one-turn α-helical segment consisting of residues Ala 44-Val 48 that connects the (C-terminal) Fe_4S_4 cluster to the (N-terminal) Fe_3S_4 cluster (cf. Figure 2). Its symmetry-related N-terminal equivalent, connecting the Fe_3S_4 to the Fe_4S_4 cluster, is present as one turn of a 3_{10} helix comprising residues Val 17-Val 19. These secondary structure elements form a highly conserved $(\beta\alpha\beta)_2$ protein fold with pseudo-2-fold symmetry that binds the two iron−sulfur cubane clusters in all dicluster ferredoxins (*5*, *65* and references therein).

The most prominent element of secondary structure in *Bs* Fd is found outside of the core fold ligating the clusters and consists of a four-turn α-helix at the C-terminus comprising residues Glu 62-Phe 75. It is very well defined (see Figure 4) and can be immediately delineated from the typical pattern of sequential and medium-range NOEs (HN-HN, Hα-HN (i, $i + 3$), and Hα-Hβ (i, $i + 3$) connectivities; Figure 2). As far as its position in the tertiary structure is concerned, it packs against the central part of the $(\beta\alpha\beta)_2$ core fold on the surface of the protein that is opposite to the clusters. It lies roughly perpendicular to the N-terminal strand of β-sheet 1 and to the C-terminal strand of β-sheet 2 with the side chain of Asn 71 buried from the solvent between the two β-sheets as clearly indicated by the slow exchange of its side chain amide protons.

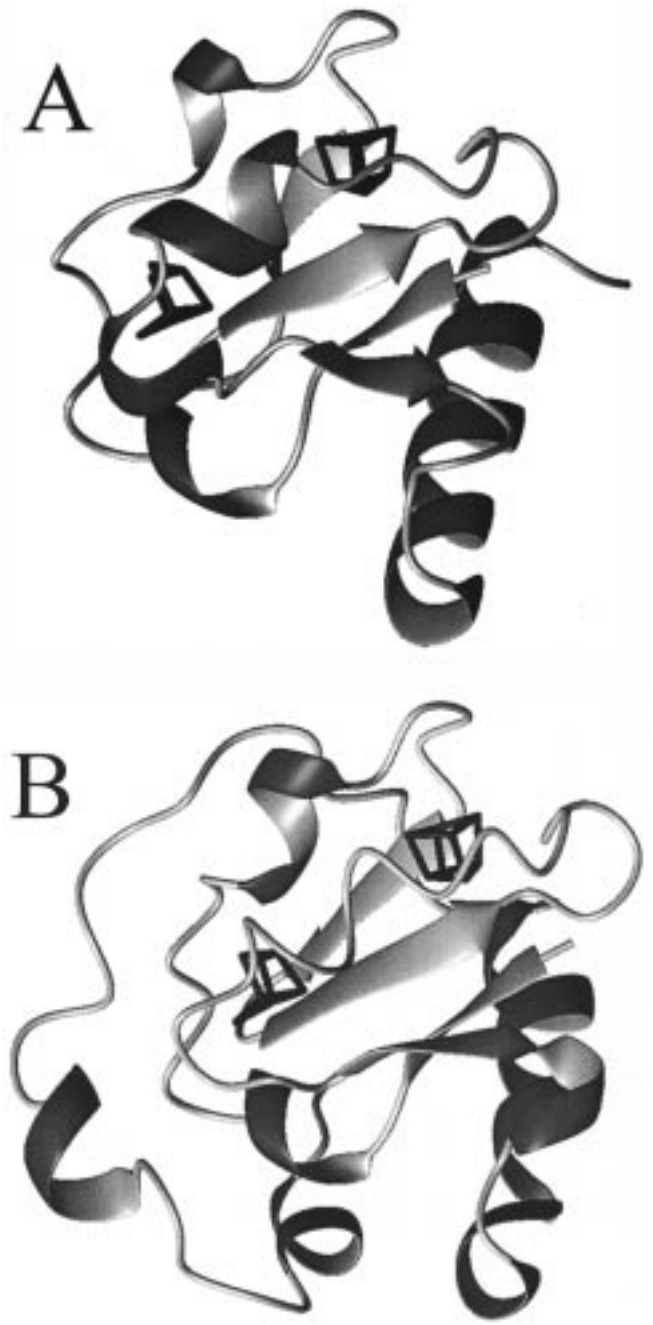

FIGURE 6: (A) Backbone representation of the energy minimized mean solution structure of *B. schlegelii* Fe_7S_8 ferredoxin showing the secondary structural elements and the two iron−sulfur clusters. (B) The same as A for the crystal structure of *A. vinelandii* ferredoxin I. The two structures have been oriented in the same way by superimposing the backbone atoms of residues 2−74. The figure was prepared with the program MOLMOL (*62*).

DISCUSSION

Sequence Comparison with Other Fe_7S_8 Ferredoxins. Table 4 shows a sequence alignment of various *Av*-type bacterial Fe_7S_8 ferredoxins (numbering system of *Av* FdI). The first three sequences are of ferredoxins from thermophilic bacteria (*B. schlegelii*, *Alicyclobacillus acidocaldarius* (formerly *Bacillus acidocaldarius*), and *Thermus thermophilus*), whereas all other sequences are from mesophilic organisms. The highest similarity to *Bs* Fd is observed for *A. acidocaldarius* Fd. Interestingly, the ferredoxins from all three thermophilic organisms lack a stretch of approximately 30 residues at the C-terminus that is characteristic for all other *Av*-type Fds.

The sequences reported in Table 4 can be divided into two groups. In the first one, which comprises *Bs* Fd and five more sequences, the loop containing the first two cysteines of the Fe_3S_4 cluster is preceded by a proline (PCXXXXXXXC), whereas in the second group (consisting of the last five sequences in Table 4) this loop is preceded by an asparagine (NCXXXXXXXC). In the second group very little variability of the residues in this loop is observed: five of the seven residues between the two binding cysteines are conserved. In particular, Asp 15, which is thought to play a role in the protonation of the Fe_3S_4 cluster upon one-electron reduction of the protein (*66*), is conserved. On the other hand, the first group of proteins shows no conserved residues in this region. The two groups of ferredoxins appear less different in the region of the Fe_4S_4 cluster and in the C-terminal region, although some distinct differences may still be pinpointed (e.g., for residues 25 and 50). The NMR spectra of all the ferredoxins reported in Table 4 are highly similar as far as their hyperfine-shifted resonances are concerned (*33* and references therein).

Comparison with the Crystal Structure of A. vinelandii [Fe_7S_8] Ferredoxin. *Av* FdI is a 106 amino acid protein that is considered to be the prototype of a whole class of bacterial Fe_7S_8 ferredoxins. Several crystal structures of the wild-type and of mutant proteins have been reported (e.g., refs *1*−*4*). Thirty-eight out of the first 77 amino acids of *Av* FdI are identical to residues in the *Bs* Fd sequence (Table 4). The pairwise backbone RMSD between the crystal structure of *Av* FdI (Protein Data Bank entry 5fd1) and the mean solution structure of *Bs* Fd is 1.42 Å for a superposition of residues 2−74, in agreement with the expected highly similar fold of the two proteins (for an overlay excluding the unrestrained residues Lys 12-Ser 15 in the NMR structure, this value is 1.36 Å). Figure 6B shows a ribbon display of the *Av* FdI structure, oriented as *Bs* Fd in Figure 6A.

At the level of secondary structure elements, some differences between the two structures can be discerned (Table 5). The short helix connecting Cys 16 to the distant ligand of the Fe_4S_4 cluster (Cys 20) is a four-residue α-helix in the case of *Av* FdI (Cys 16-Val 19) and a three-residue 3_{10} helix (Val 17-Val 19) in the *Bs* Fd solution structure. Whether this is a real structural difference cannot be assessed unambiguously due to the relatively high RMSD of Val 17-Glu 18 and the lack of medium-range NOEs in this sequential stretch. The C-terminal equivalent of this helix is recognized by MOLMOL (*62*) as a five-residue α-helix (Ala 44-Val 48) in the mean solution structure of *Bs* Fd; however it is not present in the *Av* FdI structure where Ala 47 in *Bs* Fd is replaced by a proline. The turn following the distant ligand of the Fe_3S_4 cluster (Cys 49) and comprising residues Pro 50-Ser 52 adopts a 3_{10} helical conformation in the *Bs* Fd solution structure. Due to the local maximum of the backbone RMSD for residues 50−52 (Figure 4), this feature is excluded from further discussion. The C-terminal helix of *Bs* Fd (Glu 62-Phe 75) is a four-turn α-helix whereas the corresponding helix in *Av* FdI consists of one turn of 3_{10} helix (Glu 62-Gln 65) followed by three α-helical turns (Glu 66-Ala 75).

Table 4: Sequence Alignment of Fe_7S_8 Ferredoxins[a]

```
                    5    10        20        30        40        50
                   *..  *.      *.* ***..  .*     * *. *.**  *   **  **
BASC       AYVITEPCIGTKDASCVEVCPVDCIHEGEDQYYIDPDVCIDCGACEAVCPVSAIYHEDF
ALIAC      PFVITSPCIGEKAADCVETCPVDAIHEGPDQYYIDPDLCIDCAACEPVCPVNAIYQEEF
THETH      PHVICEPCIGVKDQSCVEVCPVECIYDGGDQFYIHPEECIDCGACVPACPVNAIYPEED
MYCSM      TYVIAEPCVDVKDKACIEECPVDCIYEGARMLYIHPDECVDCGACEPVCPVEAIYYEDD
SACER      TYVIAEPCVDVLDKACIEECPVDCIYEGGRMLYIHPDECVDCGACEPVCPVEAIYYEDD
STRGR      TYVIAQPCVDVKDKACIEECPVDCIYEGQRSLYIHPDECVDCGACEPVCPVEAIFYEDD
RHORU      PYVVTENCIKCKYQDCVEVCPVDCFYEGENFLVINPDECIDCGVCNPECPAEAIAG---
AZOVI      AFVVTDNCIKCKYTDCVEVCPVDCFYEGPNFLVIHPDECIDCALCEPECPAQAIFSEDE
PSEST      TFVVTDNCIKCKYTDCVEVCPVDCFYEGPNFLVIHPDECIDCALCEPECPAQAIFSEDE
PSEPU      TFVVTDNCIKCKYTDCVEVCPVDCFYEGPNFLVIHPDECIDCALCEPECPAQAIFSEDE
RHOCA      TYVVTDNCIACKYTDCVEVCPVDCFYEGENTLVIHPDECIDCGVCEPECPADAIRPDTE

                   60        70        80        90        100   106
                             *
BASC       VPEEWKSYIQKNRDFFKK----------------------------------------
ALIAC      VPEDEKEFIEKNRNFFRNR---------------------------------------- 70.1
THETH      VPEQWKSYIELNAELAEIW---------------------------------------- 58.4
MYCSM      VPDQWSSYAQANADFFAELGSPGGASKVGQTDNDPQAIKDLPPQGED---------- 58.4
SACER      VPDEWAAYTKANVDFFDELGSPGGAAKVGKVDRDVEPVSSLPPQGE---------- 59.7
STRGR      TPEEWKDYYKANVEFFDDLGSPGGASKLGLIERDHPFVAGLPPQNA---------- 57.1
RHORU      ------KWLEINRKFADLWPNITRKGPALADADDWKDKPDK-TGLLSENPGKGTVCH 51.5
AZOVI      VPEDMQEFIQLNAELAEVWPNITEKKDPLPDAEDWDGVKGKLQHLER---------- 49.4
PSEST      VPEDQQEFIELNADLAEVWPNITEKKDALADAEEWDGVKDKLQYLER---------- 48.1
PSEPU      VPSGMENFIELNAELAEIWPNITERKDALPDAEEWDGKPGKIADLER---------- 45.5
RHOCA      -P-GMEDWVEFNRTYASQWPVITIKKDPMPDHKKYDGETGKREKYFSPNPGTGD--- 45.3
```

[a] The last column reports the similarity score (in percent) to the sequence of *B. schlegelii* ferredoxin. The alignment has been performed with the program CLUSTAL W (*84*). Residues conserved in all ferredoxins are marked with an asterisk, conservatively replaced amino acids with a dot. Residues conserved in the three thermostable ferredoxins are in bold. The numbering system is that of *A. vinelandii* FdI. Abbreviations for the organisms: BASC, *Bacillus schlegelii*; ALIAC, *Alicyclobacillus acidocaldarius*; THETH, *Thermus thermophilus*; MYCSM, *Mycobacterium smegatis*; SACER, *Saccharopolyspora erythraea*; STRGR, *Streptomyces griseus*; RHORU, *Rhodospirillum rubrum*; AZOVI, *Azotobacter vinelandii*; PSEST, *Pseudomonas stutzeri*; PSEPU, *Pseudomonas putida*; and RHOCA, *Rhodobacter capsulatus*. The sequence of *T. thermophilus* ferredoxin differs from that in the SWISS Protein Data Bank (accession number P03942). Oshima et al. have recently cloned and sequenced the gene encoding *T. thermophilus* ferredoxin and confirmed that the previously reported sequence (*85*) is correct with one exception: the residue at position 6 is not glutamine, but glutamate. The DNA sequence of *T. thermophilus* ferredoxin will appear in the DDBJ/EMBL/GenBank Database (personal communication).

Table 5: Secondary Structure Elements in the Crystal Structure of *A. vinelandii* Ferredoxin I (PDB Entry 5fd1) and the Average Solution Structure and the RMD Structure Family of *B. schlegelii* Ferredoxin[a]

secondary structure elements	*A. vinelandii* FdI	mean structure of *B. schlegelii* Fd	occurrence in the RMD family of *B. schlegelii* Fd
β-sheet 1	Phe 2-Val 4, Ile 54-Ser 56	Tyr 2-Val 3, Tyr 55-His 56	90%
helix 1	Asp 6-Cys 8 (3_{10})	Glu 6-Cys 8 (3_{10})	50%
helix 2	Cys 16-Val 19 (α)	Val 17-Val 19 (3_{10})	50%
β-sheet 2	Phe 25-Gly 28, Phe 31-Ile 34	Ile 25-Glu 27, Tyr 32-Ile 34	100%
helix 3		Ala 44-Val 48 (α)	95%
helix 4		Pro 50-Ser 52 (3_{10})	55%
helix 5	Glu 57-Glu 59 (3_{10})		
"C-terminal" helix	Glu 62-Gln 65 (3_{10}), Glu 66-Ala 75 (α)	Glu 62-Phe 75 (α)	100%

[a] Analysis performed by the program MOLMOL.

The position of the latter helix in the tertiary structure is highly similar in both *Bs* and *Av* Fd. The side chain of Asn 71, which is the only residue in the C-terminal helix that is conserved in all *Av*-type Fe_7S_8 ferredoxins (Table 4), points in both cases to the space between β-sheet 1 and 2. In the *Av* FdI crystal structure, its amide protons form hydrogen bonds with the carbonyl oxygen of Phe 67 and Val 4 (β-sheet 1), whereas its oxygen atom is hydrogen bonded to the backbone amide protons of Val 4 (β-sheet 1) and Ile 34 (β-sheet 2). Two of these hydrogen bonds (Asn 71 OD1 with Ile 34 HN and Tyr 67 O with the side chain amide protons of Asn 71) are also found in the *Bs* Fd solution structure. Fujii et al. recently proposed that the indirect interactions between the two β-sheets in the core ferredoxin fold could be important for its structural stability (*5*). Indeed, Val 4 and Ile 34 are conservatively replaced or conserved in all *Av*-type ferredoxins and there is always an aromatic residue in position 67 (Phe, Tyr, or Trp; Table 4). The equivalent position of Asn 71 in both structures strongly suggests that it plays the same role in *Bs* Fd and *Av* FdI.

As far as the β-sheets of the ferredoxin core fold are concerned, both of them are shorter by one residue on each

Table 6: Amino Acid Composition of *A. vinelandii* and *B. schlegelii* Fe_7S_8 Ferredoxins

amino acid	*B. schlegelii* Fd (residues 1−77)	*A. vinelandii* FdI (residues 1−77)	*A. vinelandii* FdI (residues 1−106)
Ala	5	6	7
Cys	8	9	9
Asp	8	7	11
Glu	8	11	14
Phe	3	5	5
Gly	3	1	3
His	2	1	2
Ile	7	5	6
Lys	5	2	6
Leu	0	4	7
Met	0	1	1
Asn	1	3	4
Pro	5	6	9
Gln	2	3	4
Arg	1	0	1
Ser	3	1	1
Thr	2	2	3
Val	8	8	9
Trp	1	0	2
Tyr	5	2	2

strand in *Bs* Fd than in *Av* FdI. In the case of β-sheet 2 located between the two cluster binding sequences, it is observed that residues 28−31 connecting the two strands have different orientations with respect to the β-sheet in the two structures. In the mean solution structure of *Bs* Fd these residues form a turn twisted out of the β-sheet plane, whereas it is in plane in the *Av* FdI structure and thus extending the β-sheet. The largest backbone displacement in this region is 3.8 Å for the Cα atom of residue 29 (Glu in *Bs* Fd and Pro in *Av* FdI). Even considering the local RMSD maximum for this turn in the family of *Bs* Fd structures (Figure 4), this is likely to be a real structural difference between the two proteins.

A comment is due to the positions of the two iron−sulfur clusters with regard to the protein frame in the solution structure of *Bs* Fd compared to *Av* FdI. Whereas the Fe_4S_4 clusters and their ligands are almost exactly in the same position when the two ferredoxins are superimposed on their backbone atoms, the Fe_3S_4 clusters are slightly displaced one with respect to the other. This is probably caused by the low number of structural constraints for the residues in the Fe_3S_4 cluster binding sequence. However, it is worth noting that some variability in the cluster positions is also observed among the available crystal structures of dicluster Fds after superposition of the protein backbones.

Determinants of Thermostability. A number of different properties has been claimed to be responsible for the increased stability of proteins from thermophiles with respect to temperature-sensitive homologous proteins. Some examples are the increase in the ratio between hydrophobic and hydrophilic residues (*67*), the reduction of the entropy loss upon folding due to the increased number of proline residues (*68*, *69*), the increase in arginine content relative to the arginine plus lysine content (*70*), the decrease in asparagine and glutamine content (*71*), the increased number of hydrogen bonds and/or salt bridges (*72*−*75*), and the minimization of the surface area-to-volume ratio (*76*).

From the comparison of the amino acid compositions of *Av* and *Bs* Fds (Table 6), it appears that there is no significant increase in the ratio between hydrophobic and hydrophilic amino acids in the latter Fd with respect to the former. A slight increase in the number of aromatic residues is observed in *Bs* Fd with respect to the N-terminal portion of *Av* FdI (11 vs 8). The Arg/(Arg + Lys) ratio is essentially the same in the two proteins. Both of them contain only one arginine residue. Also the so-called proline rule (*69*) does not hold in the present case, as the N-terminal portion of *Av* FdI contains a higher number of prolines than *Bs* Fd. All the above factors would point to a lower stability of *Bs* Fd with respect to *Av* FdI. The only evidence from the primary sequences, which is in agreement with the observed higher stability of *Bs* Fd, is its lower content in asparagine and glutamine residues, as it is known that irreversible denaturation may result from deamination of these amino acids at high temperatures (*71*).

In a recent paper on the 1.75 Å crystal structure of the hyperthermostable Fe_4S_4 ferredoxin from *Thermotoga maritima*, it was suggested that replacement of residues in strained conformation by glycines stabilizes the cluster-binding region in thermostable ferredoxins by a release of steric hindrance (*77*). This was based on the observation that the presence of glycines at particular positions in the cluster-binding sequence motif is conserved in thermostable Fe_4S_4 Fds; mesostable Fds have residues with much larger side chains at these positions. In the present study of Fe_7S_8 Fds, a sequence comparison leads to the same conclusion: all three thermostable Fe_7S_8 Fds (from *Bs*, *T. thermophilus*, and *A. acidocaldarius*) contain the sequence CIG where C is the first ligand to the Fe_3S_4 cluster (i.e., residue 8). The same sequence CIG is found in the equivalent position in the hyperthermostable Fe_4S_4 Fds from *T. maritima*, *Thermococcus litoralis*, and *Pyrococcus furiosus* and also in the Fe_8S_8-ferredoxin-like photosystem I subunit PsaC from the thermophilic cyanobacterium *Synechococcus elongatus*. In all mesostable Fe_7S_8 Fds the glycine at position $i + 2$ with respect to the first cluster ligating cysteine of the sequence is replaced by alanine, aspartate, or lysine (Table 4).

Particular attention has been devoted in the literature to amino acid substitutions occurring in helical or β-sheet regions (*74*, *78*, *79*). A sequence comparison of *Av* FdI and *Bs* Fd reveals that most of the observed residue substitutions occur in regions with a defined secondary structure in either protein. Indeed, only the helix spanning residues 16−19 is entirely conserved in the two systems. Overall, in the above regions the percentage of identical residues is only 42%, which compares to 59% for the regions without a defined secondary structure (including regions forming turns or β-bridges in both structures), and to the mean value for the whole sequence of 49.4% (Table 4). In particular, it is noted that the helix formed by residues 44−48, which is absent in *Av* FdI, contains two residue substitutions of the type Xaa (a generic amino acid) to Ala (at positions 44 and 47). Early studies of protein thermostability pointed to an important role for alanine residues in stabilizing α-helices (*80*, *81*). In a recent paper by Vogt et al. (*74*), the likelihood of a given residue exchange in an α-helix or in a β-strand was derived from a statistical analysis of residue exchanges occurring in helical or β-sheet regions in a group of 16 families of proteins with different thermal stability. The comparison of the residue exchanges observed in the present case with the above statistical results does not reveal a significant trend toward statistically favored or unfavored substitutions.

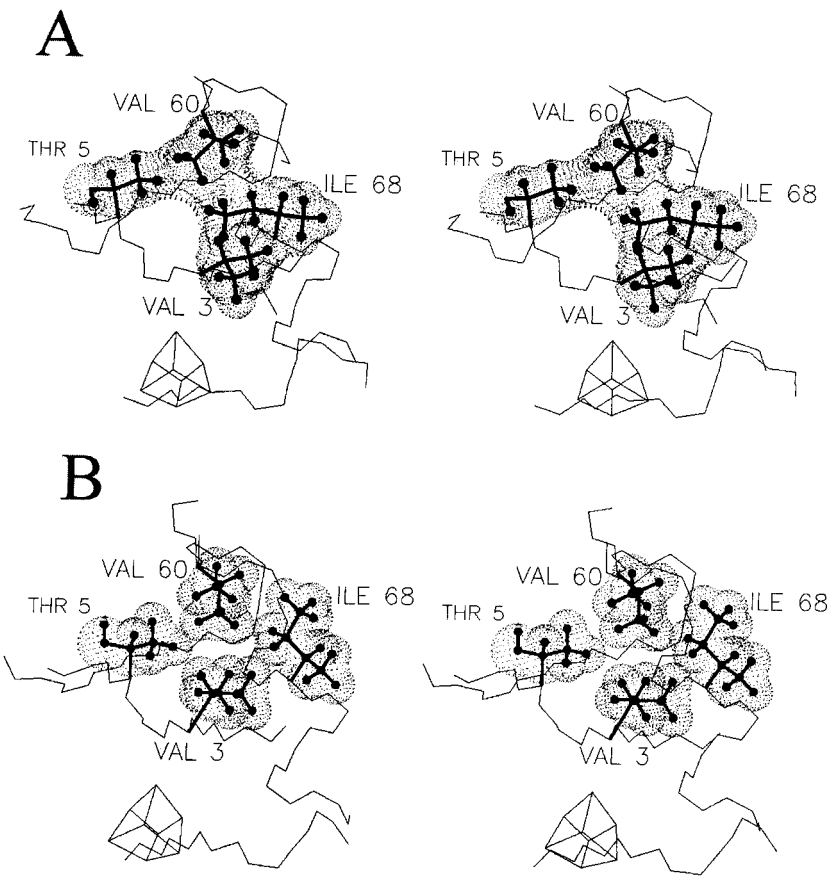

FIGURE 7: (A) A stereoview of the hydrophobic cluster formed by residues 3, 5, 60, and 68, together with the van der Waals surfaces (calculated by MOLMOL (*62*)) of the side chains. The backbone of the residues within 10 Å from the C_α atoms of Val 3 and the Fe_4S_4 cluster are also shown. (B) The same as A for the crystal structure of *A. vinelandii* ferredoxin I.

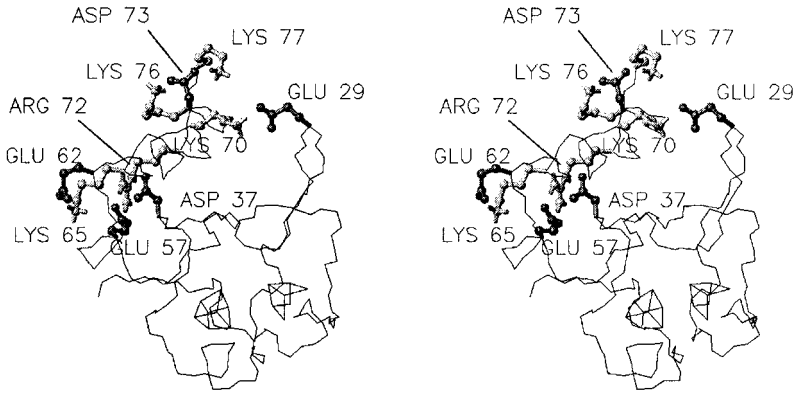

FIGURE 8: Salt bridges observed in the mean solution structure of *B. schlegelii* Fe_7S_8 ferredoxin (stereoview). Positively charged amino acids are in light gray and negatively charged ones in dark gray. The figure was prepared with the program MOLMOL (*62*).

Salt bridges, hydrogen bond networks, and hydrophobic contacts have been indicated as key factors in enhancing the thermal stability of a protein (*73*). In the present solution structure a strong interaction among hydrophobic side chains belonging to the first β-sheet and the C-terminal helix is observed. The side chain of Ile 68 is tightly packed between the side chains of Val 3 and Val 60 (the distance CG1 60 − CD1 68 is 3.7 Å, the distance CD1 68 − CG1 3 is 3.5 Å). Furthermore, the methyl group of Thr 5 is close to the CG2 atom of Val 60 (3.4 Å). This valine residue is thus packed between Ile 68 and Thr 5 (Figure 7A). It is noted that Val 3 and Val 60 (with the exception of *Streptomyces griseus* Fd) are conserved in all Fe_7S_8 Fds (Table 4). In the structure of *Av* FdI, the above interaction is not present, as the side chain of Ile 68 is pointing away from Val 3 and Val 60 (Figure 7B). This comparison is meaningful, as the RMSD values for residues 3, 5, 60, and 68 in the RMD family of *Bs* Fd are very low (average values: 0.24 ± 0.04 for the backbone and 0.33 ± 0.13 for the heavy atoms).

Bs Fd contains six salt bridges in the well-defined regions of its structure, which are listed in Table 7 and displayed in Figure 8. *Av* FdI contains four salt bridges, only one of which involves a pair of residues belonging to the sequential stretch 1−77 (i.e., to the region of *Av* FdI which aligns with the sequence of *Bs* Fd). The number of salt bridges per residue is doubled in *Bs* Fd with respect to *Av* FdI. This difference in the number of salt bridges could account by itself for a 10−20 K increase in the denaturation temperature

Table 7: Salt Bridges in the Average Solution Structure and in the RMD Family of *B. schlegelii* Ferredoxin[a]

salt bridge in the mean structure	occurrence in the RMD family[b]
Glu 29−Lys 70	100%
Asp 37−Arg 72	70%
Glu 57−Arg 72	90%
Glu 62 -Lys 65	75%
Asp 73−Lys 76	70%
Asp 73−Lys 77	50%

[a] The second column reports the percentage of structures in the RMD family where the given salt bridge is present. [b] This figure includes all salt bridges between the two residues in column one, regardless of the exchange of the terminal oxygen atoms in Asp and Glu, or of the terminal nitrogen atoms in Arg possibly occurring in the RMD family. Salt bridges in which both terminal atoms of a Asp, Glu, or Arg residue are within 4.0 Å from their partner are counted only once (e.g., only one salt bridge is counted if both terminal oxygens of an Asp are within 4.0 Å from the terminal nitrogen of a Lys).

of the protein (*74*, *75*). The only salt bridge of *Av* FdI which could be common to the present system is formed by Lys 12 and Glu 27. Of the 10 residues involved in the formation of salt bridges in the present system, only three are conserved in *Av* FdI. None of the salt bridges found in the *Bs* Fd solution structure could be present in the *Av* FdI. Finally, it is noted that all salt bridges found in *Bs* Fd involve the C-terminal helix; three of these interactions contribute to the fixation of the helix with respect to the ferredoxin core fold.

The number of hydrogen bonds in the present system is roughly the same as that in *Av* FdI. There are 29 backbone hydrogen bonds that occur in 10 or more structures of the *Bs* Fd family, which compares to 31 in *Av* FdI. Twenty of these hydrogen bonds are common to both structures. Some additional hydrogen bonds are observed for the side chain of Tyr 2 (whose hydroxyl proton is hydrogen bonded to the side chain of Glu 46), Thr 5 (whose hydroxyl proton is bonded to the carbonyl oxygen of Ala 53), and Glu 6 (whose side chain oxygen atoms make a hydrogen bond to the hydroxyl proton of Tyr 67). Such interactions are expected to stabilize the packing of the N-terminus of *Bs* Fd against the protein core. Thr 5 is kept in a position favorable for hydrogen bonding to Ala 53 by the above-mentioned interaction of its methyl group with Val 60.

Finally, it should be noted that the stretch of 30 residues at the C-terminus which is present in *Av* FdI, and is lacking in *Bs* Fd, protects the Fe_3S_4 cluster from the solvent. Therefore, this cluster is more accessible to solvent in the latter protein. Its solvent accessibility is comparable to that measured for the crystal structure of *Av* FdI after the above-mentioned 30 residues have been removed. Thus, at variance with the case of high potential ferredoxins (HiPIPs) (*82*, *83*), shielding of the iron−sulfur cluster from the solvent does not seem to play a major role for protein stabilization in Fe_3S_4 cluster containing ferredoxins.

CONCLUDING REMARKS

In this work an extensive assignment of ^{1}H resonances for the thermostable Fe_7S_8 ferredoxin from *B. schlegelii* was obtained (79% of all expected resonances). NOESY cross-peaks (1248) were assigned and integrated, giving 966 meaningful upper distance limits for DYANA structure calculations. These were complemented by 84 upper and lower distance limits used to define the structure of the two iron−sulfur centers and 47 distance constraints derived from hydrogen bonds. Four dihedral angle constraints were obtained from the hyperfine shifts of the βCH_2 protons of the cysteines coordinating to the $[Fe_4S_4]^{2+}$ cluster; in addition, a newly introduced parametrization for the hyperfine shifts of the $[Fe_3S_4]^{+}$ cluster provided another two dihedral angle constraints for two of its ligating cysteines (Cys 16 and Cys 49). With all these constraints, the solution structure of *Bs* Fd has been solved to a satisfactory degree of resolution. Only the surface loop between the first two cysteines coordinating to the Fe_3S_4 cluster remains poorly defined by the present data.

The well-defined regions of the *Bs* Fd structure were compared to the crystal structure of the homologous FdI from the mesophile *Av*, thus providing insight into the reasons for its high thermal stability. It has been shown that residue exchanges between thermostable and mesostable proteins most often occur in secondary structure elements, rather than in regions with turn or coil conformation. It can be hypothesized that such residue exchanges are tuned in order to make the secondary structure of the protein particularly stable, or to create favorable interactions between different regions of the protein. From the three-dimensional structure, otained here by NMR, it is evident that both hydrophobic and hydrophilic interactions are important in determining the high thermal stability of *Bs* Fd. Most of such interactions stabilize the N- and C- termini of the polypeptide chain and link them tightly to the core of the protein. The N-terminus of the protein is packed against the core of the protein through the hydrophobic interaction of the side chains of Val 3 and Thr 5 with the side chains of Val 60 and Ile 68. Furthermore, the side chains of residues 2, 5, and 6 are hydrogen bonded to residues 46, 53, and 67, respectively. For the C-terminal α-helix, the stabilization of the structure is ensured by six salt bridges, three of which link the helix to the core of the protein.

SUPPORTING INFORMATION AVAILABLE

Table S1 containing ^{1}H NMR resonance assignments of the oxidized Fe_7S_8 ferredoxin from *B. schlegelii* at 298 K and Figure S1 showing 1D NOE difference spectra on its hyperfine-shifted resonances in D_2O solution (6 pages). Ordering information is given on any current masthead page.

REFERENCES

1. Stout, G. H., Turley, S., Sieker, L. C., and Jensen, L. H. (1988) *Proc. Natl. Acad. Sci. U.S.A. 85*, 1020−1022.
2. Stout, C. D. (1989) *J. Mol. Biol. 205*, 545−555.
3. Shen, B., Jollie, D. R., Diller, T. C., Stout, C. D., Stephens, P. J., and Burgess, B. K. (1995) *Proc. Natl. Acad. Sci. U.S.A. 92*, 10064−10068.
4. Kemper, M. A., Stout, C. D., Lloyd, S. E. J., Prasad, G. S., Fawcett, S., Armstrong, F. A., Shen, B., and Burgess, B. K. (1997) *J. Biol. Chem. 272*, 15620−15627.
5. Fujii, T., Hata, Y., Oozeki, M., Moriyama, H., Wakagi, T., Tanaka, N., and Oshima, T. (1997) *Biochemistry 36*, 1505−1513.
6. Saeki, K., Suetsugu, K., Miyake, Y., Young, D. A., Marrs, B. L., and Matsubara, H. (1991) *J. Biol. Chem. 266*, 12889−12895.
7. Isas, J. M., Yannone, S. M., and Burgess, B. K. (1995) *J. Biol. Chem. 270*, 21258−21263.

8. Yannone, S. M., and Burgess, B. K. (1997) *J. Biol. Chem. 272*, 14454−14458.
9. Isas, J. M., and Burgess, B. K. (1994) *J. Biol. Chem. 269*, 19404−19409.
10. Morgan, T. V., Lundell, D. J., and Burgess, B. K. (1988) *J. Biol. Chem. 263*, 1370−1375.
11. Aono, S., Fukuda, N., and Okura, I. (1995) *J. Mol. Catal. A: Chemical 95*, 173−178.
12. Macedo, A. L., Moura, I., Moura, J. J. G., LeGall, J., and Huynh, B. H. (1993) *Inorg. Chem. 32*, 1101−1105.
13. Macedo, A. L., Palma, P. N., Moura, I., LeGall, J., Wray, V., and Moura, J. J. G. (1993) *Magn. Reson. Chem. 31*, S59−S67.
14. Busse, S. C., La Mar, G. N., Yu, L. P., Howard, J. B., Smith, E. T., Zhou, Z. H., and Adams, M. W. W. (1992) *Biochemistry 31*, 11952−11962.
15. Donaire, A., Gorst, C. M., Zhou, Z. H., Adams, M. W. W., and La Mar, G. N. (1994) *J. Am. Chem. Soc. 116*, 6841−6849.
16. Calzolai, L., Gorst, C. M., Zhao, Z. H., Teng, Q., Adams, M. W. W., and La Mar, G. N. (1995) *Biochemistry 34*, 11373−11384.
17. Calzolai, L., Gorst, C. M., Bren, K. L., Zhou, Z.-H., Adams, M. W. W., and La Mar, G. N. (1997) *J. Am. Chem. Soc. 119*, 9341−9350.
18. Banci, L., Bertini, I., and Luchinat, C. (1990) *Struct. Bonding 72*, 113−135.
19. Banci, L., Bertini, I., Briganti, F., and Luchinat, C. (1991) *New J. Chem. 15*, 467−477.
20. Bertini, I., Ciurli, S., and Luchinat, C. (1995) *Struct. Bonding 83*, 1−54.
21. Capozzi, F., Ciurli, S., and Luchinat, C. (1998) *Struct. Bonding 90*, 127−160.
22. Bertini, I., Luchinat, C., and Rosato, A. (1996) *Prog. Biophys. Mol. Biol. 66*, 43−80.
23. Wang, P. L., Donaire, A., Zhou, Z. H., Adams, M. W. W., and La Mar, G. N. (1996) *Biochemistry 35*, 11319−11328.
24. Hatanaka, H., Tanimura, R., Katoh, S., and Inagaki, F. (1997) *J. Mol. Biol. 268*, 922−933.
25. Nagayama, K., Ohmori, D., Imai, Y., and Oshima, T. (1983) *FEBS Lett. 158*, 208−212.
26. Nagayama, K., Imai, Y., Ohmori, D., and Oshima, T. (1984) *FEBS Lett. 169*, 79−84.
27. Nagayama, K., Ohmori, D., Imai, Y., and Oshima, T. (1986) in *Iron−Sulfur Protein Research* (Matsubara, H., Ed.) pp 125−138, Springer-Verlag, Berlin.
28. Sweeney, W. V. (1981) *J. Biol. Chem. 256*, 12222−12227.
29. Cheng, H., Grohmann, K., and Sweeney, W. V. (1992) *J. Biol. Chem. 267*, 8073−8080.
30. Cheng, H., Grohmann, K., and Sweeney, W. V. (1990) *J. Biol. Chem. 265*, 12388−12392.
31. Bentrop, D., Bertini, I., Luchinat, C., Mendes, J., Piccioli, M., and Teixeira, M. (1996) *Eur. J. Biochem. 236*, 92−99.
32. Aono, S., Bertini, I., Cowan, J. A., Luchinat, C., Rosato, A., and Viezzoli, M. S. (1996) *JBIC, J. Biol. Inorg. Chem. 1*, 523−528.
33. Bertini, I., Dikiy, A., Luchinat, C., Macinai, R., Viezzoli, M. S., and Vincenzini, M. (1997) *Biochemistry 36*, 3570−3579.
34. Bertini, I., Donaire, A., Feinberg, B. A., Luchinat, C., Piccioli, M., and Yuan, H. (1995) *Eur. J. Biochem. 232*, 192−205.
35. Aono, S., Nakamura, S., Aono, R., and Okura, I. (1994) *Biochem. Biophys. Res. Commun. 201*, 938−942.
36. Johnson, R. D., Ramaprasad, S., and La Mar, G. N. (1983) *J. Am. Chem. Soc. 105*, 7205−7206.
37. Banci, L., Bertini, I., Luchinat, C., Piccioli, M., Scozzafava, A., and Turano, P. (1989) *Inorg. Chem. 28*, 4650−4656.
38. Bax, A., and Davis, D. G. (1985) *J. Magn. Reson. 65*, 355−360.
39. Griesinger, C., Otting, G., Wüthrich, K., and Ernst, R. R. (1988) *J. Am. Chem. Soc. 110*, 7870−7872.
40. Wider, G., Macura, S., Kumar, A., Ernst, R. R., and Wüthrich, K. (1984) *J. Magn. Reson. 56*, 207−234.
41. Rance, M., Sørensen, O. W., Bodenhausen, G., Wagner, G., Ernst, R. R., and Wüthrich, K. (1983) *Biochem. Biophys. Res. Commun. 117*, 479.
42. Marion, D., and Wüthrich, K. (1983) *Biochem. Biophys. Res. Commun. 113*, 967−974.
43. Sklenar, V., Piotto, M., Leppik, R., and Saudek, V. (1993) *J. Magn. Reson., Ser. A 102*, 241−245.
44. Eccles, C., Güntert, P., Billeter, M., and Wüthrich, K. (1991) *J. Biomol. NMR 1*, 111−130.
45. Güntert, P., Mumenthaler, C., and Wüthrich, K. (1997) *J. Mol. Biol. 273*, 283−298.
46. Güntert, P., Braun, W., and Wüthrich, K. (1991) *J. Mol. Biol. 217*, 517−530.
47. Wüthrich, K. (1986) *NMR of Proteins and Nucleic Acids*, Wiley, New York.
48. Bertini, I., and Luchinat, C. (1996) *Coord. Chem. Rev. 150*, 1−300.
49. Stokes, G. (1956) *Trans. Cambridge Philos. Soc. 9*, 5.
50. Einstein, A. (1956) *Investigations on the Theory of the Brownian Movement*, Dover, New York.
51. Borgias, B., Thomas, P. D., and James, T. L. (1989) *Complete Relaxation Matrix Analysis (CORMA)*, University of California, San Francisco.
52. Banci, L., Bertini, I., Eltis, L. D., Felli, I. C., Kastrau, D. H. W., Luchinat, C., Piccioli, M., Pierattelli, R., and Smith, M. (1994) *Eur. J. Biochem. 225*, 715−725.
53. Kissinger, C. R., Sieker, L. C., Adman, E. T., and Jensen, L. H. (1991) *J. Mol. Biol. 219*, 693−715.
54. Stout, C. D. (1993) *J. Biol. Chem. 268*, 25920−25927.
55. Bertini, I., Capozzi, F., Luchinat, C., Piccioli, M., and Vila, A. J. (1994) *J. Am. Chem. Soc. 116*, 651−660.
56. Davy, S. L., Osborne, J. M., Breton, J., Moore, G. R., Thomson, A. J., Bertini, I., and Luchinat, C. (1995) *FEBS Lett. 363*, 199−204.
57. Pearlman, D. A., and Case, D. A. (1991) *SANDER*, University of California, San Francisco.
58. Pearlman, D. A., Case, D. A., Caldwell, J. W., Ross, W. S., Cheatham, T. E., Ferguson, D. M., Seibel, G. L., Singh, U. C., Weiner, P. K., and Kollman, P. A. (1995) *AMBER 4.1*, University of California, San Francisco.
59. Mouesca, J.-M., Chen, J. L., Noodleman, L., Bashford, D., and Case, D. A. (1994) *J. Am. Chem. Soc. 116*, 11898−11914.
60. Berendsen, H. J. C., Postma, J. P. M., van Gunsteren, W. F., DiNola, A., and Haak, J. R. (1984) *J. Chem. Phys. 81*, 3684−3690.
61. van Gunsteren, W. F., and Berendsen, H. J. C. (1977) *Mol. Phys. 34*, 1311−1327.
62. Koradi, R., Billeter, M., and Wüthrich, K. (1996) *J. Mol. Graphics 14*, 51−55.
63. Huber, J. G., Gaillard, J., and Moulis, J.-M. (1995) *Biochemistry 34*, 194−205.
64. Laskowski, R. A., Rullmann, J. A. C., MacArthur, M. W., Kaptein, R., and Thornton, J. M. (1996) *J. Biomol. NMR 8*, 477−486.
65. Moulis, J.-M., Sieker, L. C., Wilson, K. S., and Dauter, Z. (1996) *Protein Sci. 5*, 1765−1775.
66. Shen, B., Martin, L. L., Butt, J. N., Armstrong, F. A., Stout, C. D., Jensen, G. M., Stephens, P. J., La Mar, G. N., Gorst, C. M., and Burgess, B. K. (1993) *J. Biol. Chem. 268*, 25928−25939.
67. Haney, P., Konisky, J., Koretke, K. K., Luthey-Schulten, Z., and Wolynes, P. G. (1997) *Proteins: Struct., Funct., Genet. 28*, 117−130.
68. Matthews, B. W., Nicholson, H., and Becktel, W. J. (1987) *Proc. Natl. Acad. Sci. U.S.A. 84*, 6663−6667.
69. Watanabe, K., Chishiro, K., Kitamura, K., and Suzuki, Y. (1991) *J. Biol. Chem. 266*, 24287−24294.
70. Mrabet, N. T., Van de Broeck, A., Van den Brande, I., Stanssens, P., Laroche, Y., Lambeir, A. M., Matthijssens, G., Jenkins, J., Chiadmi, M., Van Tilbeurgh, H., Rey, F., Janin, J., Quax, W. J., Lasters, I., Maeyer, M. D., and Wodak, S. J. (1992) *Biochemistry 31*, 2253.
71. Ahern, T. J., and Klibanov, A. M. (1985) *Science 228*, 1280−1284.
72. Perutz, M. F., and Raidt, H. (1975) *Nature 255*, 256−259.
73. Querol, E., Perez-Pons, J. A., and Mozo-Villarias, A. (1996) *Protein Eng. 9*, 265−271.

74. Vogt, G., Woell, S., and Argos, P. (1997) *J. Mol. Biol. 269*, 631−643.
75. Vogt, G., and Argos, P. (1997) *Folding Des. 2*, S40−S46.
76. Chan, M. K., Mukund, S., Kletzin, A., Adams, M. W. W., and Rees, D. C. (1995) *Science 267*, 1463−1469.
77. Macedo-Ribeiro, S., Darimont, B., Sterner, R., and Huber, R. (1996) *Structure 4*, 1291−1301.
78. Angstrom, J., Moore, G. M., and Williams, R. J. P. (1982) *Biochim. Biophys. Acta 703*, 87−94.
79. Serrano, L., Sancho, J., Hirshberg, M., and Fersht, A. R. (1992) *J. Mol. Biol. 227*, 544−559.
80. Menéndez-Arias, L., and Argos, P. (1989) *J. Mol. Biol. 206*, 397−406.
81. Kelly, C. A., Nishiyama, M., Ohnishi, Y., Beppu, T., and Birktoft, J. J. (1993) *Biochemistry 32*, 3913−3922.
82. Bian, S., Hille, C. R., Hemman, C., and Cowan, J. A. (1996) *Biochemistry 35*, 14544−14552.
83. Agarwal, A., Li, D., and Cowan, J. A. (1995) *Proc. Natl. Acad. Sci. U.S.A. 92*, 9440−9444.
84. Thompson, J. D., Higgins, D. G., and Gibson, T. J. (1994) *Nucleic Acids Res. 22*, 4673−4680.
85. Sato, S., Nakazawa, K., Honnami, K., and Oshima, T. (1981) *Biochim. Biophys. Acta 668*, 277−289.

BI972818B